*Int. J. Solids Structures* Vol. 26, No. 3, pp. 271–297, 1990
Printed in Great Britain.

0020–7683/90 $3.00+.00


# A MODEL OF FILAMENT-WOUND THIN CYLINDERS

EMILIO P. CALIUS and GEORGE S. SPRINGER
Department of Aeronautics and Astronautics, Stanford University,
Stanford, CA 94305, U.S.A.

(*Received* 8 *February* 1989)

**Abstract**—A model was developed for simulating the manufacturing process of filament-wound cylinders made of a thermoset matrix composite. The model relates the process variables (winding speed, fiber tension, applied temperature) to the parameters characterizing the composite cylinder and the mandrel. The model is applicable to cylinders for which the diameter is large compared to the wall thickness. The model was implemented by a user-friendly computer code suitable for generating numerical results. The model and the corresponding code provide the following information as a function of time and position inside the composite cylinder and the mandrel during the winding and the subsequent oven curing: (i) temperature throughout the cylinder and mandrel, (ii) degree of cure throughout the cylinder, (iii) viscosity throughout the cylinder, (iv) fiber positions, (v) fiber tensions, (vi) stresses and strains throughout the cylinder and mandrel, and (vii) porosity throughout the cylinder.

## 1. INTRODUCTION

The manufacture of a part by filament winding consists of three major steps. The first step is the design of the part itself. The second step is the placement of the fibers in their appropriate positions. The third step is the selection and control of the processing conditions used during the manufacturing process. This investigation is addressed to the last point, namely to the selection of the processing conditions.

The conditions existing during the manufacturing process are governed by the following process variables: the winding speed, winding tension, and either the applied temperature or the applied heating. The appropriate values of these process variables must be employed to ensure that the filament-wound part has the required properties and dimensions.

The best way to establish the proper process variables is through a set of analytical models. In this paper a model suitable for simulating the filament-winding process is described. Verification of the model by tests, and the use of models in selecting the process variables are presented in Calius *et al.* (1989) and Lee and Springer (1989), respectively.

## 2. PROBLEM STATEMENT

The cylinder is built up by depositing bands of resin-impregnated fiber bundles onto a mandrel of outer radius $R$ and length $L$. The cylinder is a thin shell with uniform thickness in the axial and circumferential directions. This thickness varies with time during the manufacturing process. The mandrel is represented by a thin hollow cylinder with a uniform "effective" wall thickness. The thermal and mechanical effects associated with the ends of the cylinder and the mandrel are neglected. Accordingly, both the cylinder and the mandrel are treated as very long axisymmetrical bodies of equal length $L$, whose geometrical and material properties do not vary along either the axial or the circumferential directions. Hence the instantaneous temperature, viscosity, degree of cure, fiber position and tension, and stresses and strains are assumed to vary only along the radial dimension.

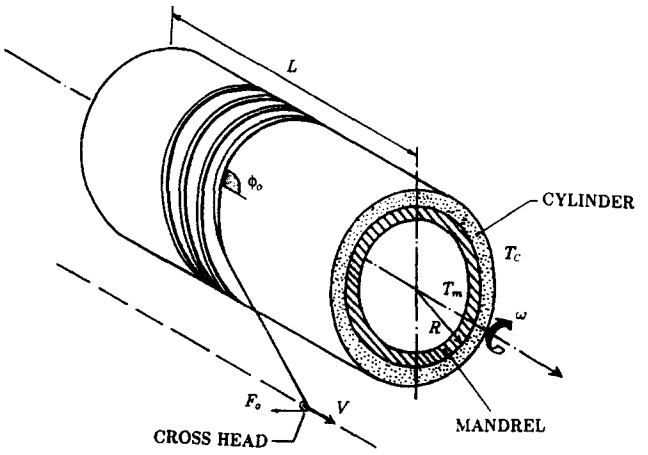


Fig. 1. Description of the problem geometry.

The winding mechanism maintains an initial tension $F_0$ in the band and an initial winding angle $\phi_0$ as the bundles are delivered onto the mandrel (Fig. 1). The fibers may be impregnated during the course of the winding by feeding them through a resin bath before they reach the mandrel (wet winding), or may be preimpregnated with resin prior to the start of the winding. The fiber bundles are deposited by a cross-head moving back and forth on a path parallel to the mandrel axis with a speed $V$, while the mandrel rotates at angular velocity $\omega$.

During winding the inner surface of the mandrel and the outer surface of the cylinder may be at room temperature, or at temperatures which are higher or lower than room temperature. Higher temperatures may arise if the cylinder is heated during winding. Lower temperatures may occur if the winding is interrupted and the cylinder is stored. Subsequent to winding (or possibly even during winding) the composite is cured by applying heat to the mandrel–cylinder assembly. The heat applied to the mandrel and cylinder surfaces (and consequently the temperatures of these surfaces $T_m$ and $T_c$, Fig. 1) may be different.

Our objective is to develop a model which relates the process variables: winding speed ($V$ and w), fiber tension ($F_0$), and surface temperatures ($T_m$ and $T_c$) to the following parameters:

(i) temperature throughout the cylinder and mandrel,
(ii) degree of cure throughout the cylinder,
(iii) viscosity throughout the cylinder,
(iv) fiber positions,
(v) fiber tensions,
(vi) stresses and strains throughout the cylinder and mandrel,
(vii) porosity throughout the cylinder, and
(viii) strength of the cylinder.

Following the scheme previously used for simulating the autoclave curing of laminates (Springer, 1983; Loos and Springer, 1983), the filament winding model consists of five submodels: thermochemical, fiber motion, stress–strain, void and strength. The thermochemical, void and strength submodels are similar to those developed for autoclave cure, and hence are discussed only briefly. The fiber motion and stress–strain submodels are markedly different from those used for flat laminates, and are described in detail.

## 3. THERMOCHEMICAL SUBMODEL

The thermochemical submodel relates the applied surface temperatures $T_m$ and $T_c$ to the temperature, degree of cure, and viscosity inside the composite. The starting point of

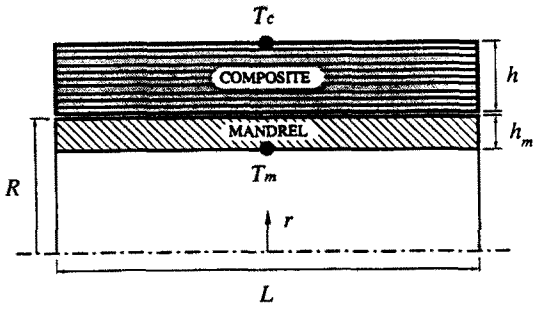


Fig. 2. Geometry of the cylinder and the mandrel, and the temperature at the inner surface of the mandrel $T_m$ and at the outer surface of the cylinder $T_c$.

this submodel is the conservation of energy which, for the axisymmetric one-dimensional problem being considered, can be written as (Eckert and Drake, 1972)

$$\rho C\frac{\partial T}{\partial t}=\frac{1}{r}\frac{\partial}{\partial r}\left(r\kappa\frac{\partial T}{\partial r}\right)+\rho\dot{H} \tag{1}$$

where $T$ is the temperature inside the composite and the mandrel, $t$ is time, and $r$ is the radial coordinate (Fig.2). $\dot{H}$ is the rate at which heat is generated or absorbed by chemical reactions, $\rho$ is the density, $\kappa$ is the transverse thermal conductivity, and $C$ is the specific heat of the composite.

The degree of cure $\alpha$ of the composite is defined as (Loos and Springer, 1983)

$$\alpha=H/H_r \tag{2}$$

where $H$ is the heat which has evolved from the start of the reaction (at time $t=t_0$) to the present time, and $H_r$ is the total heat of reaction. As for $t_0$, it is the time at which the material element under consideration became part of the cylinder.

From eqn (2) we obtain an expression for $\dot{H}$

$$\dot{H}=\left(\frac{\mathrm{d}\alpha}{\mathrm{d}t}\right)H_r \tag{3}$$

where $\mathrm{d}\alpha/\mathrm{d}t$ is the rate of degree of cure. Substitution of eqn (3) into eqn (1) yields

$$\rho C\frac{\partial T}{\partial t}=\frac{1}{r}\frac{\partial}{\partial r}\left(r\kappa\frac{\partial T}{\partial r}\right)+\rho H_r\frac{\mathrm{d}\alpha}{\mathrm{d}t}. \tag{4}$$

Equation (4) contains two unknowns, the temperature $T$ and the degree of cure $\alpha$. Therefore, an additional expression is needed which contains these two parameters. This expression, which represents the chemical kinetics, can symbolically be written as

$$\frac{\mathrm{d}\alpha}{\mathrm{d}t}=f_1(\alpha,t). \tag{5}$$

Expressions for $f_1$ for Hercules 3501-6 and Fiberite 976 epoxy resins are given in Lee *et al.* (1982) and Dusi *et al.* (1987), respectively, and for Hercules HBRF-55 resin in Calius *et al.* (1989) and Bhi *et al.* (1987).

The density $\rho$, the thermal conductivity $\kappa$, and the heat capacity $C$ may vary as the cure reaction proceeds. Expressions relating these properties to the temperature and degree of cure are given in Appendix A.

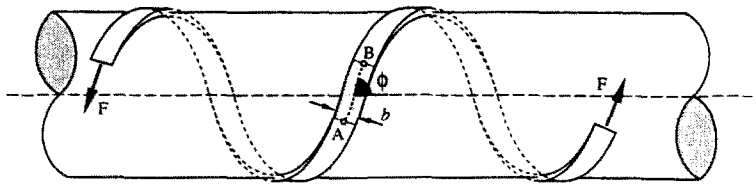


Fig. 3. Illustration of a resin-impregnated fiber band.

As initial conditions, the initial temperature $T_0$ and the initial degree of cure of the material $\alpha_0$ must be specified at the time $t_0$ at which the material is added to the cylinder. Hence, the initial conditions can be expressed as

$$T = T_0 \quad \alpha = \alpha_0 \quad \text{at } t = t_0. \tag{6}$$

$T_0$ may be but does not have to be the same as the temperature $T_a$ of the room where the winding is taking place, while $\alpha_0$ is the degree of cure the resin has acquired while waiting to be placed on the cylinder. Since the cylinder's thickness is built up gradually, $t_0$ is dfferent for each layer.

The boundary conditions require that the temperature on the inner surface of the mandrel $T_m$ and at the outer surface of the cylinder $T_c$ be specified at all times. Thus, the temperature boundary conditions are

$$\left.\begin{aligned} T &= T_c \quad \text{at } r = R+h \\ T &= T_m \quad \text{at } r = R-h_m \end{aligned}\right\} \quad t > 0. \tag{7}$$

$R$ is the outer radius of the mandrel and $h$ is the thickness of the cylinder (Fig. 2). During winding the cylinder outer surface temperature $T_c$ frequently approximates the ambient room temperature $T_a$. During cure $T_c$ is the temperature resulting from the applied heating. In the latter case $T_c$ is likely to be different from the ambient air temperature. Note that $h$ varies with time, while $h_m$, which is the effective thermal thickness of the mandrel, remains constant throughout the winding process.

Solutions to eqns (4)–(7) provide the temperature $T$ and the degree of cure $\alpha$ as functions of position and time inside the cylinder.

Once the temperature $T$ and the degree of cure $\alpha$ are known the resin viscosity can be calculated from an expression of the form

$$\mu = f_2(\alpha, T). \tag{8}$$

Expressions of this function for Hercules 3501-6 and Fiberite 976 epoxy resins are also presented in Lee *et al.* (1982) and Dusi *et al.* (1987), respectively, and for Hercules HBRF-55 epoxy resin in Calius *et al.* (1989) and Bhi *et al.* (1987).

## 4. FIBER MOTION SUBMODEL

The resin-impregnated fiber bundles (tows) are wound side-by-side, forming a band of approximately rectangular cross-section with width $b$ and thickness $\Delta h$ (Fig. 3). This band is wound into successive layers. Initially (at time $t = t_0$) the fiber tension in the band is $F_0$ and the fiber's winding angle is $\phi_0$. During processing the fibers may move, precipitating a change in the fiber tension and in the fiber angle. The instantaneous (at time $t > t_0$) fiber tension and fiber angle are denoted by $F$ and $\phi$, respectively (Fig. 3).

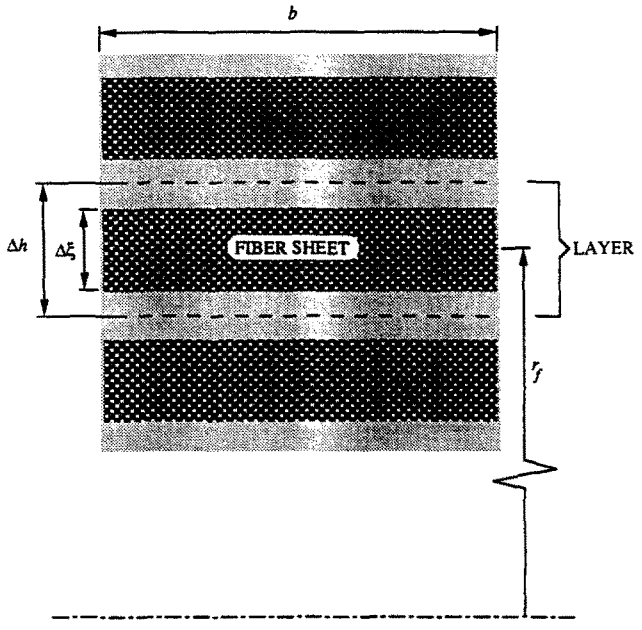


Fig. 4. Idealization of the fiber sheets in the fiber motion submodel.

To simplify the analysis we treat a large number of fibers as a unit. These fibers make up what we call a fiber sheet (Fig. 4). A fiber sheet (of thickness $\Delta\xi$) includes all of the fibers in a rectangular cross-section whose width is the same as that of the band. All of the fibers in a fiber sheet are assumed to moved together.

The fibers may move in the axial, hoop and radial directions. However, only the radial components of the fiber tension are not self-equilibrating since the tension is constant along the fibers. Consequently, we are most concerned with the motion of the fibers through the resin in the radial direction. This movement is described by the instantaneous radial position $r_f$ of the fiber sheet's midsurface (Fig. 5). Changes in the radial position may arise for three reasons:

(i) the curvature of the fibers gives rise to a radial component of the fiber tension inducing fiber motion in the radial direction (Fig. 5b);
(ii) the dimensions of the mandrel may change during processing resulting in movement of every layer in the composite (Fig. 5c);

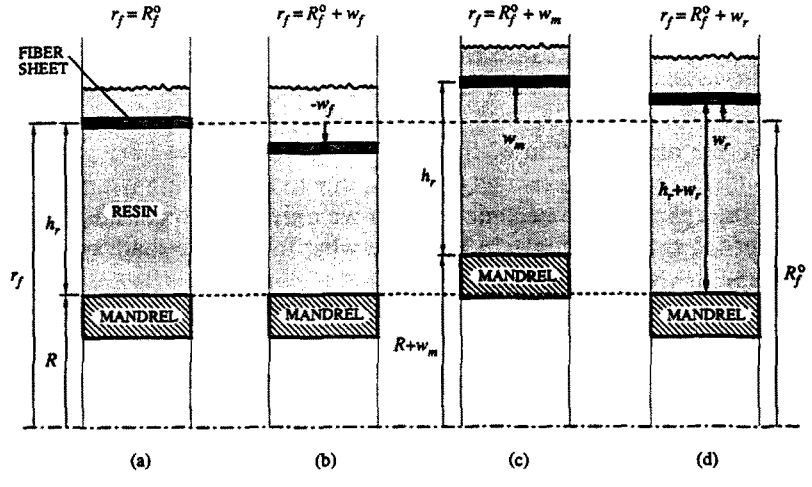


Fig. 5. Illustration of the changes in fiber position relative to cylinder's axis from its position at the time of winding (a), due to the winding tension (b), due to deformation of the mandrel (c), and due to changes in resin density (d).

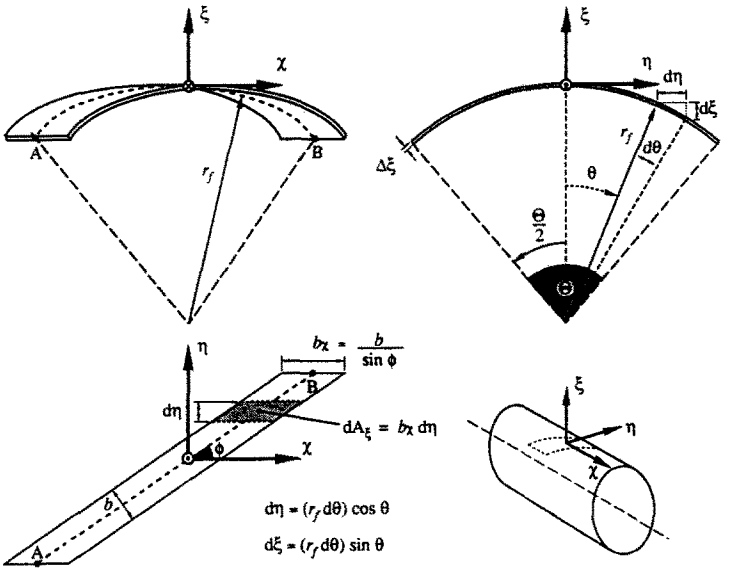


Fig. 6. Geometry of the AB fiber band segment.

(iii) the resin surrounding the fibers may expand or contract, causing radial motion of the fibers (Fig. 5d).

Thus the instantaneous radial position $r_f$ of a fiber sheet's midsurface can be written as

$$r_f = R_f^0 + w_f + w_m + w_r \tag{9}$$

where $R_f^0$ is the radial position of the fiber sheet at time $t_0$, $w_f$ is the radial displacement of the fiber sheet relative to the surrounding resin, $w_m$ is the radial displacement of the sheet due to mandrel deformation, and $w_r$ is the radial displacement of the sheet due to resin density changes caused by changes in the resin's temperature, degree of cure or moisture content.

The objective of this submodel is to develop an equation which can be solved for $w_f$ at each instant of time. The effects of (ii) and (iii) which result in $w_m$ and $w_r$ are dealt with in the next section.

In developing this submodel it is assumed that all the fibers in a given layer start moving at the same time. This assumption implies that in each layer the band appears instantaneously in its place at the designated time $t_0$. This is a reasonable assumption for the cylinders considered here because the time required to wind any given band into a complete layer is negligible compared to the total time involved in winding the entire cylinder.

To calculate the radial motion of the fiber sheet, we take the fiber path around the cylinder to be sufficiently long so that edge effects, due to fibers being wrapped around the end closures of the cylinder, are negligible. Then we only need to consider an arbitrarily chosen portion of the sheet, as shown in Fig. 3. In what follows we shall concern ourselves with a short segment AB of a fiber sheet.

*Equilibrium*

For the AB segment we choose a local Cartesian coordinate system $\xi$, $\chi$, $\eta$ attached to the center of the segment (Fig. 6). $\xi$ is perpendicular to the surface of the sheet, $\chi$ is parallel to the axis of the cylinder, and $\eta$ is perpendicular to $\xi$–$\chi$ plane.

The total fiber tensions acting at each end of the segment are denoted by $F^A$ and $F^B$ (Fig. 7). $F_\chi$ and $F_\Omega$ are the axial and circumferential components of this force. At each of the endpoints $F_\Omega$ can be further decomposed into $F_\xi$ and $F_\eta$, which are the force components acting in the $\xi$ and $\eta$ directions.

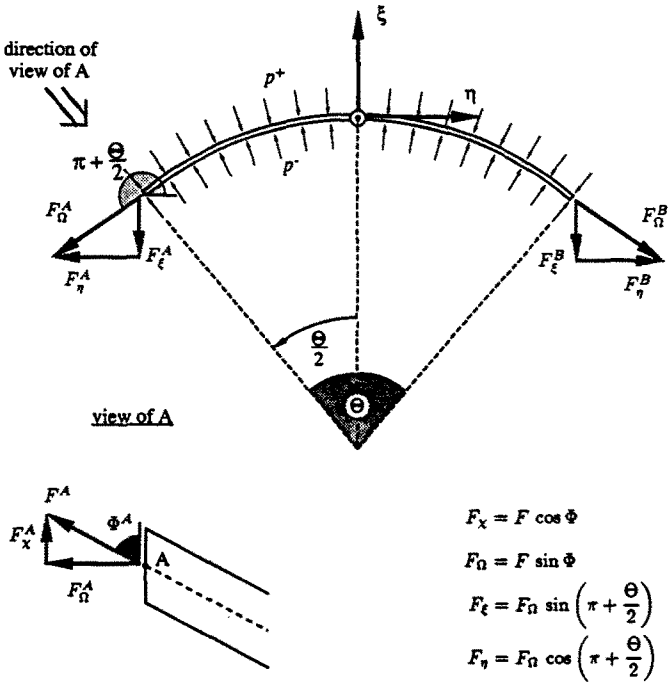


Fig. 7. Forces acting on the AB fiber band segment.

There are also pressure forces acting on the inner and outer surfaces of the fiber sheet due to the pressure in the resin (Fig. 7). The force balance in the $\xi$ direction is

$$F_\xi^A + F_\xi^B + \int_{\mathscr{A}_\xi} p^- \, d\mathscr{A}_\xi - \int_{\mathscr{A}_\xi} p^+ \, d\mathscr{A}_\xi = 0 \tag{10}$$

where $p^+$ and $p^-$ are the pressures on the outside and inside of this sheet, respectively. $d\mathscr{A}_\xi$ is an element of the projected fiber sheet are perpendicular to the $\xi$ axis over which the pressure acts. From Fig. 6, given that $b$ is a constant, this area is

$$d\mathscr{A}_\xi = b_\chi \, d\eta = b_\chi r_f \cos\theta \, d\theta \tag{11}$$

where $b_\chi$ is the projection along the $\chi$ axis of the sheet's width $b$, and $r_f$ is the radial position of the sheet's midsurface. $\theta$ is the circumferential angle between the origin of the coordinate system and the edge of the element $d\mathscr{A}_\xi$. Since the fiber sheet is very thin, in writing eqn (11) we have taken the radius of the upper and lower surfaces to be the same as that of the midsurface. Thus the integral of the pressure over the surface area can be written as

$$\int_{\mathscr{A}_\xi} P \, d\mathscr{A}_\xi = b_\chi \int_{-\Theta/2}^{\Theta/2} P r_f \cos\theta \, d\theta \tag{12}$$

where $\Theta/2$ is the circumferential angle between the origin of the coordinate system and the segment's end points A and B.

By taking the pressure $P$ and the radial position $r_f$ of the midsurface to be constant over this segment, eqn (12) can be integrated to yield

$$\int_{\mathscr{A}_\xi} P \, \mathrm{d}\mathscr{A}_\xi = Pb_\chi r_f \left[ \sin\left(\frac{\Theta}{2}\right) - \sin\left(-\frac{\Theta}{2}\right) \right] = 2P\left(\frac{b}{\sin\phi}\right) r_f \sin\frac{\Theta}{2}. \tag{13}$$

The second equality was obtained by replacing $b_\chi$ with its projection $b/\sin\phi$, where $\phi$ is the instantaneous band angle (Fig. 6).

The $\xi$ components of the fiber tension can be expressed in terms of the total fiber tension $F$. By referring to the free body diagram in Fig. 7, we can write

$$F_\xi^A = (F_\Omega^A) \sin\left(\pi + \frac{\Theta}{2}\right) = (F^A \sin \Phi^A)\left[-\sin\left(\frac{\Theta}{2}\right)\right]$$

$$F_\xi^B = (F_\Omega^B) \sin\left(-\frac{\Theta}{2}\right) = (F^B \sin \Phi^B)\left[\sin\left(-\frac{\Theta}{2}\right)\right] \tag{14}$$

where $F_\Omega$ is the circumferential component of the tension, and $\Phi$ is the angle between the total tension and its axial component at the end of the segment. The superscripts A and B refer to these end points.

It seems reasonable to assume that the shear forces between the fibers and the resin are negligible in comparison with the fiber tension. Under this assumption the axial components of the end forces are equal ($F_\chi^A = F_\chi^B$). For the short segment AB under consideration, we have also taken the pressure distribution to be uniform and symmetric about the $\chi$ axis. A consequence of this assumption is that the normal components of the end forces are also equal ($F_\xi^A = F_\xi^B$). The above-mentioned force equalities imply that $F_\Omega^A$ is equal to $F_\Omega^B$ [see eqn (14)]. From Fig. 7 it can now be seen that if $F_\chi^A = F_\chi^B$ and $F_\Omega^A = F_\Omega^B$ then at the two ends of the segment the total forces $F^A$ and $F^B$ are equal, and the angles $\Phi^A$ and $\Phi^B$ are equal

$$F^A = F^B = F$$

$$\Phi^A = \Phi^B = \phi. \tag{15}$$

Since the total fiber tension $F$ has the same magnitude and direction at both A and B, the angle $\Phi$ between the force and the $\chi$ axis is the same as the fiber band angle $\phi$. This equality is indicated in the second of eqn (15). We may now write eqn (14) as

$$F_\xi^A = F_\xi^B = -2(F \sin\phi) \sin\frac{\Theta}{2}. \tag{16}$$

By substituting eqns (13) and (16) into (10) we obtain the following form of the equilibrium equation

$$-F \sin^2\phi + (p^- + p^+) b r_f = 0. \tag{17}$$

*Resin flow*

The fiber sheet under consideration is actually not a solid, but a close-packed assemblage of fibers. Resin can flow relative to the fibers through the interstices between these fibers. The radial forces pull the fibers through the resin in the radial direction with a velocity $\dot{w}_f$. In practice $\dot{w}_f$ is low and the resin's viscosity $\mu$ is high so that the flow is laminar. By modeling the fiber sheet as a porous medium, the fiber velocity can be related to the pressure drop through Darcy's law (Daily and Harleman, 1966; Collins, 1961), which we write as

$$p^+ - p^- = \Delta\xi\left(\frac{\mu}{\mathscr{S}}\right)\dot{w}_f \tag{18}$$

where $\mu$ is the resin viscosity, $\mathscr{S}$ is the sheet's permeability, and $\Delta\xi$ is the distance through which the pressure drop takes place, which is the fiber sheet's thickness. We define $\Delta\xi$ as the thickness of the band times the fiber volume fraction $v_f$

$$\Delta\xi = v_f \Delta h. \tag{19}$$

The permeability can be deduced from data or can be approximated by the Carman–Kozeny formula (Happel, 1959). Equations (17) and (18) together yield a relation between the radial fiber tension and fiber velocity. However, since the fiber tension itself is not constant but changes with fiber position, additional relations are necessary to define the problem.

*Fiber tension*

The force $F$ can be expressed in terms of the fiber stress through the boundary traction at each end of the segment AB

$$F = \int_{\mathscr{A}_f} \sigma_f \, d\mathscr{A}_f = \bar{\sigma}_f \mathscr{A}_f \tag{20}$$

where $\sigma_f$ is the axial fiber stress, $\bar{\sigma}_f$ is the average axial fiber sheet stress, and $\mathscr{A}_f$ is the total cross-sectional area of all the fibers at the end of the segment.

By assuming that the stress distribution is uniform and that the fibers behave in a linearly elastic manner we may apply Hooke's law as follows

$$\varepsilon_f \simeq \left(\frac{\bar{\sigma}_f}{E^f_{11}} - 2\nu^f_{12}\frac{\sigma_p}{E^f_{22}}\right) + \overset{T}{\varepsilon}_f \tag{21}$$

where $\varepsilon_f$ is the total fiber strain and $\overset{T}{\varepsilon}_f$ is the thermal strain along the fiber axis. $E^f_{11}$ and $E^f_{22}$ are the fibers' longitudinal and transverse Young's moduli, and $\nu^f_{12}$ is its longitudinal Poisson ratio. $\sigma_p$ is the fiber stress in the direction perpendicular to the fiber axis, arising from the radial pressures $p^+$ and $p^-$. Henceforth we neglect this transverse stress because it is of secondary interest in comparison with the longitudinal stress. Equation (21) can thus be rewritten as

$$\bar{\sigma}_f = E^f_{11}(\varepsilon_f - \overset{T}{\varepsilon}_f). \tag{22}$$

Initially (at winding time) the fiber tension is $F_0$ and the corresponding average fiber sheet stress along the fiber axis is $\bar{\sigma}_{f_0}$

$$F_0 = \bar{\sigma}_{f_0}\mathscr{A}_f \tag{23}$$

By combining eqns (20) and (23), the instantaneous fiber tension $F$ may be expressed in terms of the change in stress from the time the band was wound ($t = t_0$) to the present time $t$:

$$F = F_0 + (\bar{\sigma}_f - \bar{\sigma}_{f_0})\mathscr{A}_f. \tag{24}$$

To write eqn (24) above, we assumed that the area of the fiber sheet's cross-section remains essentially constant throughout the process. From Fig. 4, given that $b$ and $\Delta\xi$ are constant over this segment, this cross-sectional area is

$$\mathscr{A}_f = b\Delta\xi \tag{25}$$

where $\Delta\xi$ corresponds to the thickness of the fiber sheet.

By using eqn (22) we can write

$$\bar{\sigma}_f - \bar{\sigma}_{f_0} = E^f_{11}[(\varepsilon_f - \varepsilon_{f_0}) + (\overset{T}{\varepsilon}_f - \overset{T}{\varepsilon}_{f_0})] \tag{26}$$

where $\varepsilon_{f_0}$ is the longitudinal fiber strain and $\overset{T}{\varepsilon}_{f_0}$ is the longitudinal thermal strain at winding time. For fibers whose thermal strain varies linearly with temperature we have

$$\overset{T}{\varepsilon}_f - \overset{T}{\varepsilon}_{f_0} = \beta^f_{11} T - \beta^f_{11} T_0 \tag{27}$$

where $\beta^f_{11}$ is the fiber's longitudinal coefficient of thermal expansion, $T$ is the instantaneous fiber temperature and $T_0$ is the fiber temperature at winding time. The temperature usually varies with radial position, so the thermal strain may change as the fiber sheet moves even if $T$ does not change as time passes.

By combining eqn (17) with eqn (18) and eqns (24)–(27) we may express the radial equilibrium equation in the following form

$$\dot{w}_f + \frac{1}{r_f}\left(\frac{\mathscr{P}}{\mu}\right)\{E^f_{11}[(\varepsilon_f - \varepsilon_{f_0}) + \beta^f_{11}(T - T_0)]\}\sin^2\phi + \left(\frac{1}{b\Delta\xi r_f}\right)\left(\frac{\mathscr{P}}{\mu}\right)F_0 \sin^2\phi = 0. \tag{28}$$

In order to complete our definition of this model we must express the fiber strains in terms of the fiber sheet's position.

*Strain–position relation*

The change in the longitudinal fiber strain is defined as

$$\varepsilon_f - \varepsilon_{f_0} = \left(\frac{l_f - l_0}{l_0}\right) - \left(\frac{l^0_f - l_0}{l_0}\right) \tag{29}$$

where $l_0$ is the original length of the fibers in the segment before the winding tension is applied, and $l^0_f$ and $l_f$ are the fiber lengths under tension at the winding time $t_0$ and at time $t$, respectively.

Since the strains caused by the winding tension are small, such that $l_0 \simeq l^0_f$, we may write

$$\varepsilon_f - \varepsilon_{f_0} \simeq \frac{l_f - l^0_f}{l^0_f}. \tag{30}$$

Based on the geometry shown in Fig. 8, these lengths may be expressed as

$$l_f = \sqrt{(\Delta\chi + \Delta u)^2 + (r_f\Theta)^2}$$
$$l^0_f = \sqrt{\Delta\chi^2 + (R^0_f\Theta)^2} \tag{31}$$

where $\Delta\chi$ is the axial distance between the endpoints of the segment, and $\Delta u$ is the difference in axial displacements $u$ of the two endpoints of the segment. $\Theta$ is the circumferential angle between these endpoints.

For small displacements the axial component of the fibers' stretching or shrinkage may be approximated by

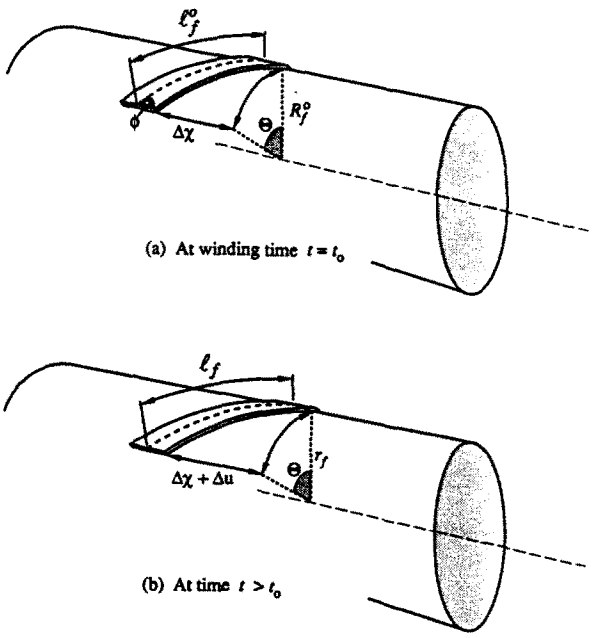


Fig. 8. Length of the fibers in the AB segment.

$$\Delta u \simeq \left(\frac{\partial u}{\partial \chi}\right)\Delta\chi. \tag{32}$$

Geometric considerations provide the relationship between the axial and circumferential components of the length ($\Delta\chi$ and $R_f^0\Theta$) and the winding angle $\phi_0$ (Fig. 8)

$$\frac{R_f^0\Theta}{\Delta\chi} = \tan\phi_0. \tag{33}$$

By combining eqns (31)–(33), after algebraic manipulations, we obtain

$$l_f = r_f\Theta\sqrt{\left(\frac{1+(\partial u/\partial\chi)}{(r_f/R_f^0)}\right)^2\frac{1}{\tan^2\phi_0}+1}$$

$$l_f^0 = R_f^0\Theta\sqrt{\frac{1}{\tan^2\phi_0}+1}. \tag{34}$$

Substitution of eqn (34) into eqn (30) yields

$$\varepsilon_f - \varepsilon_{f_0} \simeq \left(\frac{r_f}{R_f^0}\right)\sqrt{\frac{(1/\tan^2\phi_0)\left(\dfrac{1+(\partial u/\partial\chi)}{r_f/R_f^0}\right)^2+1}{(1/\tan^2\phi_0)+1}}-1. \tag{35}$$

*Governing equation*

Straightforward but space-consuming algebraic manipulations of eqns (9), (28) and (35) result in (Calius and Springer, 1989)

$$f_3\dot{w}_f+\frac{w_f}{R_f^0}\dot{w}_f+f_2\frac{w_f^2}{R_f^{0^2}}+f_1\frac{w_f}{R_f^0}+f_0=0. \tag{36}$$

The parameters $f_0$ through $f_3$ are

$$f_0=C\left\{\frac{F_0}{E_{11}^f b\Delta\xi}-\beta_{11}^f(T-T_0)+\frac{w}{R_f^0}+\frac{1}{2}\left[\left(1+\frac{\partial u}{\partial\chi}\right)^2-\left(1+\frac{w}{R_f^0}\right)\right]\cos^2\phi_0\right\}\sin^2\phi_0$$

$$f_1=C\left\{1-\frac{1}{2}\left[1+\left(1+\frac{\partial u}{\partial\chi}\right)^2\left(1-2\frac{w}{R_f^0}\right)\right]\cos^2\phi_0\right\}\sin^2\phi_0$$

$$f_2=C\left\{\frac{1}{2}\left(1+\frac{\partial u}{\partial\chi}\right)^2\cos^2\phi_0\right\}\sin^2\phi_0$$

$$f_3=1+\frac{w}{R_f^0} \tag{37}$$

where $C$ and w are defined as

$$w=w_m+w_r \qquad C=\frac{1}{R_f^0}\left(\frac{\mathscr{S}}{\mu}\right)E_{11}^f. \tag{38}$$

Solutions to eqn (36) provide $w_f$. In order to perform the calculations, expressions are needed for the band rotation $\partial u/\partial\chi$, the displacement w, and the temperature $T$. The appropriate relationships for the first two are derived in the next chapter. The last one is, of course, provided by the thermochemical model described in the previous chapter. All other geometrical and material parameters are known.

Equation (36) may be simplified to (Appendix B)

$$g_3^t\Delta\dot{w}_f+\frac{g_1^t}{R_f^0}\Delta w_f+g_0^t=0 \tag{39}$$

where

$$g_0^t=(f_3^t-f_3^{t-\Delta t})\dot{w}_f^{t-\Delta t}+(f_2^t-f_2^{t-\Delta t})\frac{w_f^{t-\Delta t^2}}{R_f^{0^2}}+(f_1^t-f_1^{t-\Delta t})\frac{w_f^{t-\Delta t}}{R_f^0}+(f_0^t-f_0^{t-\Delta t})$$
$$-f_3^t\dot{w}_f^{t-\Delta t}-\frac{w_f^{t-\Delta t}}{R_f^0}\dot{w}_f^{t-\Delta t}$$

$$g_1^t=2f_2^t\frac{w_f^{t-\Delta t}}{R_f^0}+f_1^t \quad g_2^t=f_2^t \quad g_3^t=f_3^t+\frac{w_f^{t-\Delta t}}{R_f^0}. \tag{40}$$

Equation (39) is a first-order linear ordinary differential equation whose coefficients $g_0$ through $g_3$ can be treated as constants during a small time interval. The unique solution to eqn (39) is (Boyce and DiPrima, 1977)

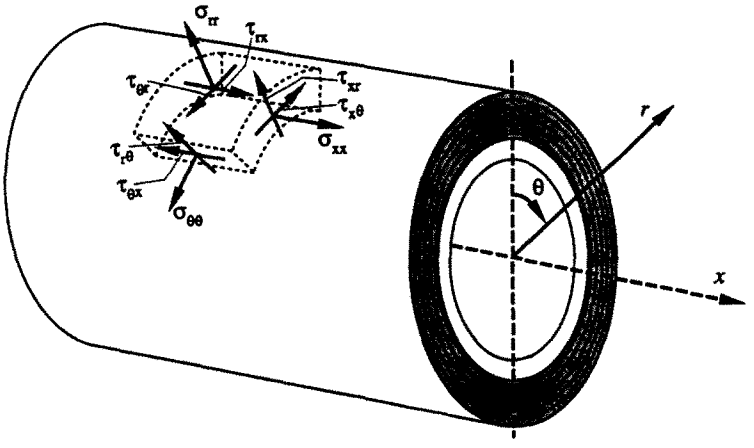


Fig. 9. Illustration of the cylinder and mandrel assembly's stress components and the coordinate system.

$$\Delta w_f = \left(\frac{g_0^t}{g_1^t}\right) R_f^0 [e^{-(g_1^t/g_3^t R_f^0)\Delta t} - 1]. \tag{41}$$

## 5. STRESS AND STRAIN SUBMODEL

*Introduction*

The stress–strain submodel provides the stresses and strains inside the cylinder as functions of position and time. This submodel was developed on the basis of the following assumptions:

(a) the normal stresses in the radial direction $\sigma_{rr}$ are negligible in comparison to the in-plane normal stresses $\sigma_{xx}$ and $\sigma_{\theta\theta}$ (Fig. 9),
(b) inertia effects are negligible,
(c) the composite winding consists of a stack of thin cylindrical layers, with each layer being composed of a single material wound at a constant fiber angle,
(d) the mandrel is either cylindrical or, for stress analysis purposes, can be idealized as an "effective" cylinder, and
(e) the stress–strain laws are uniform through the mandrel and through each layer's thickness.

Note that although the wind angle and material properties are taken to be the same everywhere within a given layer, they may vary from layer to layer.

From (a), the stress and strain components to be considered in this analysis are

$$\begin{aligned} \boldsymbol{\sigma} &= \{\sigma_{xx}, \sigma_{\theta\theta}, \tau_{xr}, \tau_{r\theta}, \tau_{\theta x}\}^{\mathscr{T}} \\ \boldsymbol{\varepsilon} &= \{\varepsilon_{xx}, \varepsilon_{\theta\theta}, \gamma_{xr}, \gamma_{r\theta}, \gamma_{\theta x}\}^{\mathscr{T}} \end{aligned} \tag{42}$$

where the $\mathscr{T}$ superscript has the conventional meaning of the transpose of the vector. $\sigma$ and $\varepsilon$ denote the normal stress and strain components, and $\tau$ and $\gamma$ denote the engineering shear stress and strain components. The subscripts $x$, $r$ and $\theta$ refer to directions defined by a cylinder-centered coordinate system (Fig. 9).

In eqn (42), $\boldsymbol{\varepsilon}$ is the total strain vector, which is the linear superposition of the mechanical (stress-induced) $\overset{\sigma}{\boldsymbol{\varepsilon}}$ and thermochemical $\overset{T}{\boldsymbol{\varepsilon}}$ strains

$$\boldsymbol{\varepsilon} = \overset{\sigma}{\boldsymbol{\varepsilon}} + \overset{T}{\boldsymbol{\varepsilon}} \tag{43}$$

where $\overset{T}{\boldsymbol{\varepsilon}}$ represents the strain due to thermochemical changes in the density of the material and may include changes due to temperature and chemical reactions (shrinkage).

The governing equations are derived from the mandrel–cylinder assembly's instantaneous energy balance through a variational procedure. The principle of minimum potential energy is chosen to provide the static equilibrium equations. This principle is expressed as (Reddy, 1985)

$$\delta_\Omega(U+W)=0 \tag{44}$$

where the operator $\delta_\Omega$ represents variation with respect to the model's unknowns, which will be discussed later. $U$ is the assembly's total strain energy functional, and $W$ is the work performed by the external applied and reaction forces acting on the cylinder and its mandrel. In the present case, the assembly is assumed to be simply-supported. Furthermore, the work performed by the winding mechanism is included in the layers' initial strain energy. Thus there are no external forces, and we have

$$W=0. \tag{45}$$

At time $t$ the total strain energy is comprised of the mandrel's strain energy $U_m^t$ and the cylinder's strain energy $U_c^t$. The latter can be further decomposed into three parts:

(i) the initial strain energy $U_0$ introduced into the cylinder by the winding tension $F_0$,
(ii) the strain energy $U_p^t$ due to deformations of the cylinder which take place during the processing up to time $t$, and
(iii) the fibers' strain energy $U_f^t$ due to the movement (up to time $t$) of the fibers within the cylinder (see Section 4).

Consequently, eqn (44) may now be rewritten as

$$\delta_\Omega(U_0+U_p^t+U_f^t+U_m^t)=0. \tag{46}$$

It is convenient to express the strain energies in terms of strain energy densities

$$\begin{aligned} U_0+U_p^t+U_f^t &= \int_{\mathcal{V}_c}(\psi_0+\psi_p^t+v_f\psi_f^t)\,\mathrm{d}\mathcal{V}_c \\ U_m^t &= \int_{\mathcal{V}_m}\psi_m^t\,\mathrm{d}\mathcal{V}_m \end{aligned} \tag{47}$$

where $\mathcal{V}_c$ and $\mathcal{V}_m$ are the volumes of the cylinder and the mandrel. $v_f$ is the composite's fiber volume fraction and is included here because $\psi_f^t$ is the strain energy of the fibers only. $\psi_0$, $\psi_p^t$, $\psi_f^t$ and $\psi_m^t$ are the strain energy densities corresponding to $U_0$, $U_p^t$, $U_f^t$ and $U_m^t$. The strain energy density is defined as

$$\psi^t \equiv \int \boldsymbol{\sigma}^t\,\mathrm{d}\boldsymbol{\varepsilon}^t \tag{48}$$

where $\boldsymbol{\sigma}^t$ and $\boldsymbol{\varepsilon}^t$ are the instantaneous stress and total strain vectors defined in eqn (42).

Since the cylinder is laminated, the strain energy's volume integral can conveniently be split among the layers. Thus the first of eqn (47) becomes

$$U_0+U_p^t+U_f^t=\int_{-L/2}^{L/2}\int_0^{2\pi}\left\{\sum_{k=1}^{N}\int_{r_k-(h_k/2)}^{r_k+(h_k/2)}[(\psi_0)_k+(\psi_p^t)_k+v_{f_k}(\psi_f^t)_k]r\,\mathrm{d}r\right\}\mathrm{d}\theta\,\mathrm{d}x. \tag{49}$$

where $L$ is the cylinder's length, $r_k$ is the midsurface radius and $h_k$ the thickness of layer

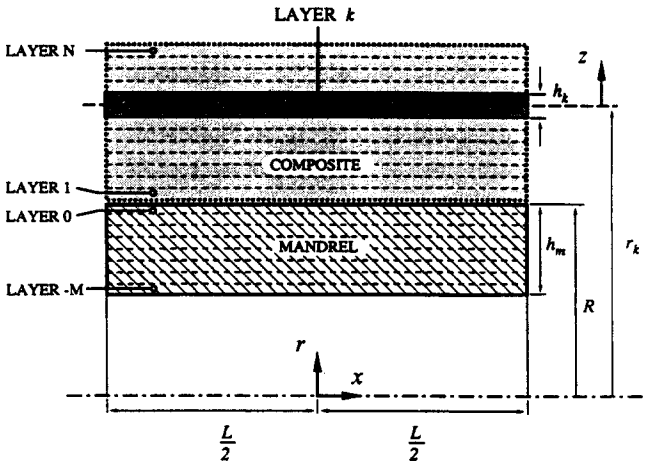


Fig. 10. Illustration of the composite layer's geometry.

number $k$ out of a laminate total of $N$. The layers are numbered from the cylinder's inner surface outwards and $k$ varies from 1 to $N$ (Fig. 10).

For a cylindrical mandrel, the second of eqn (47) can be written as

$$U_m^t = \int_{-L/2}^{L/2} \int_0^{2\pi} \int_{R-h_m}^{R} \psi_m^t r \, dr \, d\theta \, dx \tag{50}$$

where $R$ is the mandrel's outer surface radius and $h_m$ is its "effective" thickness.

It is convenient to consider the mandrel as part of the laminated cylinder. This is accomplished by treating the mandrel as a sub-laminate consisting of one or more layers within the total cylinder–mandrel assembly. Thus we write the mandrel's strain energy as

$$U_m^t = \int_{-L/2}^{L/2} \int_0^{2\pi} \left\{ \sum_{k=-M}^{0} \int_{r_k-(h_k/2)}^{r_k+(h_k/2)} [(\psi_0)_k + (\psi_p^t)_k] r \, dr \right\} d\theta \, dx \tag{51}$$

where the subscript $k$ now refers to one of the $M+1$ "layers" in the mandrel. These "layers" are numbered from the mandrel's outer surface inwards and $k$ varies from 0 to $-M$. Although there is no fiber motion energy term, we do have an initial contribution $(\psi_0)_k$ from the forces applied to the mandrel as each layer of the composite is wound.

Since the deformations are assumed to be infinitesimal, the principal dimensions of the cylinder and mandrel may be treated as constants. Then, using its commutative property (Lanczos, 1986), the variational operator can be moved inside the $U$ integral, giving the following expression for equilibrium

$$\delta_\Omega(U_0 + U_p^t + U_f^t + U_m^t) = \int_{-L/2}^{L/2} \int_0^{2\pi} \left\{ \sum_{k=1}^{N} \int_{r_k-(h_k/2)}^{r_k+(h_k/2)} \delta_\Omega [v_{f_k}(\psi_f^t)_k] r \, dr \right.$$
$$\left. + \sum_{k=-M}^{N} \int_{r_k-(h_k/2)}^{r_k+(h_k/2)} \delta_\Omega [(\psi_0)_k + (\psi_p^t)_k] r \, dr \right\} d\theta \, dx = 0. \tag{52}$$

The next step is to formulate each of the strain energy density terms in the above equation.

*Strain energy density*

In order to proceed with the analysis, we must express each of the four strain energy densities in terms of appropriate stresses and strains [eqn (48)].

The initial strain energy density $(\psi_0)_k$ due to the winding tension is a constant. Hence, the variation of $(\psi_0)_k$ is zero, and we do not need to concern ourselves with this term any further, except to note that it is assumed that the initial strain is exclusively due to the longitudinal tension of the tows.

The composite and mandrel processing strain energy density is expressed in terms of cylindrical stress and strains components, with the aid of eqn (42), as

$$(\psi_p^t)_k = \int_{(\varepsilon_{xx}^{t_0})_k}^{(\varepsilon_{xx}^t)_k} (\sigma_{xx}^t)_k \, \mathrm{d}(\varepsilon_{xx}^t)_k + \int_{(\varepsilon_{\theta\theta}^{t_0})_k}^{(\varepsilon_{\theta\theta}^t)_k} (\sigma_{\theta\theta}^t)_k \, \mathrm{d}(\varepsilon_{\theta\theta}^t)_k + \int_0^{(\gamma_{\theta r}^t)_k} (\tau_{\theta r}^t)_k \, \mathrm{d}(\gamma_{\theta r}^t)_k + \int_0^{(\gamma_{rx}^t)_k} (\tau_{rx}^t)_k \, \mathrm{d}(\gamma_{rx}^t)_k + \int_0^{(\gamma_{x\theta}^t)_k} (\tau_{x\theta}^t)_k \, \mathrm{d}(\gamma_{x\theta}^t)_k \quad (53)$$

where $(\varepsilon_{xx}^{t_0})_k$ and $(\varepsilon_{\theta\theta}^{t_0})_k$ are the initial normal strains in layer $k$ ($-M \leqslant k \leqslant N$). These strains are related to the strains parallel and perpendicular to the fibers at the time of winding ($t = t_0$) by a rotation of the reference axes (Calius and Springer, 1989)

$$\begin{aligned}
(\varepsilon_{xx}^{t_0})_k &= (\varepsilon_{\parallel}^{t_0})_k \cos^2 \phi_{ok} + (\varepsilon_{\perp}^{t_0})_k \sin^2 \phi_{0k} \\
(\varepsilon_{\theta\theta}^{t_0})_k &= (\varepsilon_{\parallel}^{t_0})_k \sin^2 \phi_{ok} + (\varepsilon_{\perp}^{t_0})_k \cos^2 \phi_{0k} \\
(\gamma_{xr}^{t_0})_k &= (\gamma_{r\theta}^{t_0})_k = (\gamma_{\theta x}^{t_0})_k = 0
\end{aligned} \quad (54)$$

where $(\varepsilon_{\parallel}^{t_0})_k$ and $(\varepsilon_{\perp}^{t_0})_k$ are the strains in the directions parallel and perpendicular to the fibers. We note that at the time of winding the strains in the layer are exclusively attributed to the applied tension $(F_0)_k$. The relationship between the strains and the applied tension is derived in next section. The lower limits of the last three integrals are set to zero because at the instant of winding, when the material is "soft", shear is neglected.

Equation (53) represents the strain energy density due to changes in the composite strain. In developing this equation it was assumed that the fibers are "locked" in the resin. In fact, as was discussed previously, the fibers may move relative to the resin. This motion introduces the following additional strain energy density in the layer

$$(\psi_f^t)_k = \int_{(\varepsilon_{xx}^t)_k}^{(\varepsilon_{fxx}^t)_k} (\sigma_{fxx}^t)_k \, \mathrm{d}(\varepsilon_{xx}^t)_k + \int_{(\varepsilon_{\theta\theta}^t)_k}^{(\varepsilon_{f\theta\theta}^t)_k} (\sigma_{f\theta\theta}^t)_k \, \mathrm{d}(\varepsilon_{\theta\theta}^t)_k \quad (55)$$

where $(\varepsilon_{fxx}^t)_k$ and $(\varepsilon_{f\theta\theta}^t)_k$ are the axial and hoop components of the total fiber strain $\varepsilon_f$ in layer $k$ at time $t$. $(\sigma_{fxx}^t)_k$ and $(\sigma_{f\theta\theta}^t)_k$ are the axial and hoop components of the fiber stress. Only normal strains and stresses are included in eqn (55) because shear in the fibers is negligible. The upper limits of the integral are the true fiber strains. The lower limits are the strains the fibers would have if they had not moved relative to the resin. These lower limits are taken to be equal to the strain of the composite at time $t$. Expressions for the fiber's stress and strain are given in the subsequent sections, along with those that apply to the composite.

In order to evaluate the above integrals we need relationships between the stresses and the total strains, i.e. we need a set of constitutive equations for each material. These are given next.

*Stress–strain relations*

There are three kinds of materials involved in the process: (i) the fibers, (ii) the composite and (iii) the mandrel.

The fiber's stress–strain relations may be described by a linearly elastic, time-independent law. The form of the relationships applicable to the fibers at any time during the process is given by eqns (4.14) and (4.19). In the $x$–$\theta$ coordinate system these are (Lubin, 1982)

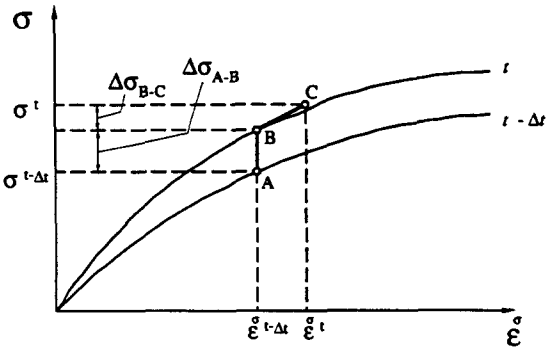


Fig. 11. Stress and mechanical strain changes during a process step.

$$(\sigma^t_{fxx})_k = (\bar{\sigma}^t_f)_k \cos^2 \phi_k = (E^f_{11})_k[(\varepsilon_f)_k - (\beta^f_{11})_k(T^t_k - T^{t_0}_k)] \cos^2 \phi_k$$
$$(\sigma^t_{f\theta\theta})_k = (\bar{\sigma}^t_f)_k \sin^2 \phi_k = (E^f_{11})_k[(\varepsilon_f)_k - (\beta^f_{11})_k(T^t_k - T^{t_0}_k)] \sin^2 \phi_k \tag{56}$$

where the $(E^f_{11})_k$ is the longitudinal Young's modulus for the fibers in layer $k$, and $(\beta^f_{11})_k$ is their coefficient of longitudinal thermal expansion. $(E^f_{11})_k$ and $(\beta^f_{11})_k$ are considered to be constant throughout the processing cycles.

The mandrel is considered to be part of the laminate, hence it is convenient to describe the mandrel's material in the same way as the composite. The differences in the mandrel and the composite's properties are accounted for by choosing the proper set of coefficients for the constitutive equations, as indicated subsequently.

During winding the stress and strain levels are low, and the winding tension $(F_0)_k$ is applied along the fiber direction. Consequently, the behavior of each band can be approximated by Hooke's law for a transversely isotropic material. Then the composite layer's initial longitudinal and transverse strains are

$$(\varepsilon^{t_0}_{\parallel})_k = (S^{t_0}_{\parallel})_k(\bar{\sigma}_0)_k \quad (\varepsilon^{t_0}_{\perp})_k = (S^{t_0}_{\perp})_k(\bar{\sigma}_0)_k \tag{57}$$

where $(S^{t_0}_{\parallel})_k$ and $(S^{t_0}_{\perp})_k$ are the composite stiffnesses at winding time. Expressions for these stiffnesses are given in Appendix C. The average stress $\bar{\sigma}_0$ is defined by

$$(\bar{\sigma}_0)_k = \frac{(F_0)_k}{b_k h_k}. \tag{58}$$

As before, $b_k$ and $h_k$ are the winding band width and thickness.

During processing the properties of the composite change, and, consequently so does the stress–strain relationship. We calculate the changes in stresses and strain which occur in each layer's stress and strain from time $t-\Delta t$ to $t$. The stress change in the $k$th layer during a time interval is taken to be composed of two increments, as illustrated in Fig. 11

$$(\Delta\sigma)^t_k = \sigma^t_k - \sigma^{t-\Delta t}_k = (\Delta\sigma_{A-B})_k + (\Delta\sigma_{B-C})_k. \tag{59}$$

In the first increment (A–B) the strain is kept constant at its value at A, and the changes in stress due to the known changes in material properties during the time interval $\Delta t$ are calculated. In the second increment (B–C) the material properties are kept constant at their value at time $t$, and the changes in stress corresponding to a change in strain $\Delta\mathring{\varepsilon}$ are found. Thus the stress in the $k$th layer is

$$\sigma^t_k = \sigma^{t-\Delta t}_k + \left[\sum_{t_i=t_0}^{t_i=t-\Delta t} \left\{\left[\frac{\partial}{\partial t}[\bar{Q}]^{t_i}_k\right]\Delta\mathring{\varepsilon}^{t_i}_k\right\}\right]\Delta t + [\bar{Q}]^t_k(\mathring{\varepsilon}^t_k - \mathring{\varepsilon}^{t-\Delta t}_k) \tag{60}$$

where $[\bar{Q}]_k^t$ is the reduced stiffness matrix of layer $k$. Expressions for $[\bar{Q}]_k^t$ for anisotropic and isotropic layers are given in Appendix C. By using the proper reduced stiffnesses for each layer in the cylinder and the mandrel, both the composite and mandrel materials are automatically included in the analysis.

The strain energy densities in the previous section were formulated in terms of total strains. Equation (43) is used to transform the stress-induced strain $\overset{\sigma}{\varepsilon}{}_k^t$ in eqn (60) into total strains. However, eqn (43) introduces additional thermochemical strains $\overset{T}{\varepsilon}{}_k^t$. The strain–temperatures relationship for the composite and the mandrel is approximated in a manner similar to that used for the stress–strain relationship. This results in

$$\overset{T}{\varepsilon}{}_k^t = \overset{T}{\varepsilon}{}_k^{t-\Delta t} + \left\{\frac{\partial}{\partial t}\boldsymbol{\beta}_k^{t-\Delta t}\right\}(T_k^{t-\Delta t} - T_k^0)\Delta t^{(j)} + \boldsymbol{\beta}_k^t(T_k^t - T_k^{t-\Delta t}) \tag{61}$$

where $T_k^0$ is the temperature at which the layer was wound. $\boldsymbol{\beta}_k$ is the vector of thermal expansion coefficients for layer $k$ (Appendix C). In writing eqn (61) $\boldsymbol{\beta}_k$ was taken to be independent of temperature. As before, eqn (61) is applicable to both the mandrel and the composite, with the substitution of the proper values in $\boldsymbol{\beta}_k$.

The time derivatives in eqns (60) and (61) may be approximated by

$$\frac{\partial}{\partial t}[\bar{Q}]_k^{t-\Delta t} = \frac{[\bar{Q}]_k^t - [\bar{Q}]_k^{t-\Delta t}}{\Delta t} \quad \frac{\partial}{\partial t}\boldsymbol{\beta}_k^{t-\Delta t} = \frac{\boldsymbol{\beta}_k^t - \boldsymbol{\beta}_k^{t-\Delta t}}{\Delta t}. \tag{62}$$

Equations (56), (60) and (61) give the stresses in terms of the total strains. By substituting these equations into eqns (55) and (53), it becomes possible to evaluate the strain energy density integrals of the previous section. The results of these integrations are the strain energy densities as functions of total strain and temperature.

*Deformation*

An approximate solution to our model requires that the distribution of either the strains or the displacements be assumed. Choosing the displacements has the advantage of automatically satisfying compatibility within each layer. Here we postulate axial $u_k^t$, hoop $v_k^t$ and radial $w_k^t$ displacements in each layer (composite or mandrel) as functions of the coordinates $x$, $\theta$, $z$ and time $t$. The coordinates $x$ and $\theta$ were defined previously (Fig. 9), while $z$ is the radial position relative to the midsurface of layer $k$, as shown in Fig. 10. Since each layer is considered to act as a thin cylinder, the displacement's $z$-coordinate dependency can be separated from the rest by using the following classic thin-section approximation (Calladine, 1986)

$$\begin{aligned} u_k^t &= \bar{u}_{k(x,\theta,t)} + z\hat{u}_{k(x,\theta,t)} \\ v_k^t &= \bar{v}_{k(x,\theta,t)} + z\hat{v}_{k(x,\theta,t)} \\ w_k^t &= \bar{w}_{k(x,\theta,t)} + z\hat{w}_{k(x,\theta,t)} \end{aligned} \tag{63}$$

where $\bar{u}_k$ and $\bar{v}_k$ are the axial and hoop displacements on the layer's midsurface, and $\bar{w}_k$ is the radial displacement of the layer's midsurface. $\hat{u}_k$ and $\hat{v}_k$ are the rotations of the axial and hoop cross-sections about the layer's midsurface. $\hat{w}_k$ is the change in the layer's thickness. This formulation implies that cross-sections initially normal to the midsurface remain plane, though not necessarily normal.

As was stated before, the cylinder–mandrel assembly is axisymmetrical, so none of the displacement functions depends on the angular coordinate $\theta$. Additionally, the radial displacement $w$ is assumed to be independent of the axial coordinate $x$. This latter approximation is reasonable because generally the mandrel is sufficiently rigid to prevent any

bending of the cylinder or the mandrel. With these approximations the simplest expressions for the parameters in eqn (63) are

$$\begin{aligned} \bar{u}_{k(x,\theta,t)} &= u'_{0k}x \quad \hat{u}_{k(x,\theta,t)} = u'_{1k}x \\ \bar{v}_{k(x,\theta,t)} &= v'_{0k}x \quad \hat{v}_{k(x,\theta,t)} = v'_{1k}x \\ \bar{w}_{k(x,\theta,t)} &= w'_{0k} \quad \hat{w}_{k(x,\theta,t)} = \frac{(\Delta w'_r)_k}{h_k} \end{aligned} \tag{64}$$

where $u'_{0k}$, $v'_{0k}$ and $w'_{0k}$, and $u'_{1k}$ and $v'_{1k}$ are undetermined coefficients which only depend on time. $(\Delta w'_k)_k$ is the change in layer thickness from the original thickness $h_k$. In the absence of the radial stress $\sigma_{rr}$ (and the resulting mechanical strain $\hat{\varepsilon}_{rr}$), this thickness change is entirely due to thermochemical density changes. Thus, by definition

$$\frac{(\Delta w'_r)_k}{h_k} = (\bar{\varepsilon}^t_{rr})_k = (\bar{\varepsilon}^{t-\Delta t}_{rr})_k + \left\{\frac{\partial}{\partial t}(\beta^{t-\Delta t}_{rr})_k\right\}(T^{t-\Delta t}_k - T^{t_{0k}}_k)\Delta t + (\beta^t_{rr})_k(T^t_k - T^{t-\Delta t}_k) \tag{65}$$

where the thermochemical radial strain $(\bar{\varepsilon}^t_{rr})_k$ is taken to behave as per eqn (61). $T^{t_{0k}}_k$ is the temperature of layer $k$ at the time $t_{0k}$ at which it was added to the winding.

Equations (63) and (64) yield the following expressions for the displacement functions

$$u^t_k = u'_{0k}x + zu'_{1k}x \quad v^t_k = v'_{0k}x + zv'_{1k}x \quad w^t_k = w'_{0k} + z(\bar{\varepsilon}^t_{rr})_k. \tag{66}$$

*Displacement constraints*

*Interlaminar compatibility.* When there are no delaminations in the cylinder, compatibility requires that the displacements of any two contiguous layers $k$ and $k-1$ match at the interface between these layers. However, we must remember that the layers are added to the cylinder at different times, and thus layers $k$ and $k-1$ may experience different amounts of total displacement. At any instant of time $t$ this condition can be expressed for the displacements proposed by eqn (66) as

$$\left.\begin{aligned} u'_{0k}x - \frac{h_k}{2}u'_{1k}x &= \left[u'_{0(k-1)}x + \frac{h_{k-1}}{2}u'_{1(k-1)}x\right] - \left\{u'^{t_{0k}}_{0(k-1)}x + \frac{h_{k-1}}{2}u'^{t_{0k}}_{1(k-1)}x\right\} \\ v'_{0k}x - \frac{h_k}{2}v'_{1k}x &= \left[v'_{0(k-1)}x + \frac{h_{k-1}}{2}v'_{1(k-1)}x\right] - \left\{v'^{t_{0k}}_{0(k-1)}x + \frac{h_{k-1}}{2}u'^{t_{0k}}_{1(k-1)}x\right\} \\ w'_{0k} - \frac{h_k}{2}(\bar{\varepsilon}^t_{rr})_k &= \left[w'_{0(k-1)} + \frac{h_{k-1}}{2}(\bar{\varepsilon}^t_{rr})_{k-1}\right] - \left\{w'^{t_{0k}}_{0(k-1)} + \frac{h_{k-1}}{2}(\bar{\varepsilon}^{t_{0k}}_{rr})_{k-1}\right\} \end{aligned}\right\}$$

$$-(M-1) \leqslant k \leqslant N \quad k \neq 1. \tag{67}$$

The terms in the square brackets on the right-hand side of eqn (67) are, at time $t$, the total axial, hoop and radial displacements of layer $k-1$ at its interface with layer $k$. The terms in the curly brackets represent what the displacements of layer $k-1$ were at the time $t = t_{0k}$ when layer $k$ was added. The terms in the curly brackets are constants at any time $t > t_{0k}$.

By applying eqn (67) recursively, we obtain the following relationships between any two non-contiguous layers designated by the subscripts $j$ and $k$

$$u^t_{0k} - \frac{h_k}{2}u^t_{1k} = \left[u^t_{0j} + \frac{h_j}{2}u^t_{1j} + \sum_{i=j+1}^{k-1} h_i u^t_{1i}\right] - \sum_{i=j+1}^{k}\left\{u^{t_{0i}}_{0(i-1)} + \frac{h_{i-1}}{2}u^{t_{0i}}_{1(i-1)}\right\}$$

$$v^t_{0k} - \frac{h_k}{2}v^t_{1k} = \left[v^t_{0j} + \frac{h_j}{2}v^t_{1j} + \sum_{i=j+1}^{k-1} h_i v^t_{1i}\right] - \sum_{i=j+1}^{k}\left\{v^{t_{0i}}_{0(i-1)} + \frac{h_{i-1}}{2}v^{t_{0i}}_{1(i-1)}\right\}$$

$$w^t_{0k} - \frac{h_k}{2}(\bar{\varepsilon}^t_{rr})_k = \left[w^t_{0j} + \frac{h_j}{2}(\bar{\varepsilon}^t_{rr})_j + \sum_{i=j+1}^{k-1} h_i(\bar{\varepsilon}^t_{rr})_i\right] - \sum_{i=j+1}^{k}\left\{w^{t_{0i}}_{0(i-1)} + \frac{h_{i-1}}{2}(\bar{\varepsilon}^{t_{0i}}_{rr})_{i-1}\right\}. \quad (68)$$

Note that the axial coordinate $x$ does not appear in eqn (68) because it cancels out in each equation. As noted in the previous paragraph, the subscripts $j$ and $k$ refer to layers, both of which must be either in the cylinder or the mandrel.

*Boundary conditions.* At the ends of the cylinder each layer is wrapped around the end closures of the mandrel. This anchors the layers so that, over a time step $\Delta t$, every layer experiences nearly the same axial displacement at the ends ($x = \pm L/2$). Thus at time $t$

$$(u^t_{0k} - u^{t-\Delta t}_{0k})\frac{L}{2} + z_k(u^t_{1k} - u^{t-\Delta t}_{1k})\frac{L}{2} = (u^t_{0j} - u^{t-\Delta t}_{0j})\frac{L}{2} + z_j(u^t_{1j} - u^{t-\Delta t}_{1j})\frac{L}{2} = \text{constant} \quad (69)$$

where $z_j$ and $z_k$ are radial positions measured with respect to the midsurfaces of layers $j$ and $k$, respectively. Unless they are in contact, eqn (69) applies to the composite and the mandrel separately. The above condition can be satisfied only if the $z$-dependent terms vanish for every layer in the cylinder and the mandrel. Thus we write

$$u^t_{1k} = u^{t-\Delta t}_{1k} \quad (70)$$

which implies that the axial cross-section rotation $u_{1k}$ is independent of time $t$.

The composite cylinder is made up of a large number of helical layer pairs and hoop layers. In our model these layers are represented by thin cylindrical shells, for which it is reasonable to assume that radial lines remain radial. This condition can be expressed as

$$\frac{(v^t_{0k} - v^{t-\Delta t}_{0k}) + z_k(v^t_{1k} - v^{t-\Delta t}_{1k})}{r_k + z_k} = \frac{(v^t_{0j} - v^{t-\Delta t}_{0j}) + z_j(v^t_{1j} - v^{t-\Delta t}_{1j})}{r_j + z_j} = \text{constant}. \quad (71)$$

This expression may be manipulated to yield

$$v^t_{1k} - v^{t-\Delta t}_{1k} = \frac{v^t_{0k} - v^{t-\Delta t}_{0k}}{r_k}. \quad (72)$$

*Initial conditions.* The initial ($t = t_{0k}$) layer displacements are

$$u^{t_{0k}}_k = 0, \quad v^{t_{0k}}_k = 0, \quad w^{t_{0k}}_k = 0. \quad (73)$$

The conditions given by eqn (73) can only be satisfied if all the coefficients on the right-hand side of eqn (66) are zero. Thus we have

$$\begin{aligned} u^{t_{0k}}_{0k} &= 0 \quad u^{t_{0k}}_{1k} = 0 \\ v^{t_{0k}}_{0k} &= 0 \quad v^{t_{0k}}_{1k} = 0. \\ w^{t_{0k}}_{0k} &= 0 \end{aligned} \quad (74)$$

Let us consider the first time step, at which $t - \Delta t = t_{0k}$. For this time step the combination of eqns (70), (72) and (74) yields

$$u^t_{1k} = 0$$

$$v^t_{1k} = \frac{v^t_{0k}}{r_k}. \tag{75}$$

It is clear from eqn (75) that axial and hoop cross-sections which were initially normal to the midsurface of the layer will remain normal throughout the processing.

*Interlaminar relations.* By combining eqns (68) and (75), we obtain the following expressions for the displacement coefficients in any layer of the composite cylinder ($1 < k \leqslant N$)

$$u^t_{0k} = u^t_{01} - \sum_{i=2}^{k} u^{t_{0i}}_{0(i-1)}$$

$$v^t_{0k} = \left(1 - \frac{h_k}{2r_k}\right)^{-1} \left[ v^t_{01} \left(1 + \frac{h_1}{2r_1}\right) \prod_{j=2}^{k-1} \left(\frac{1+(h_j/2r_j)}{1-(h_k/2r_k)}\right)\right] - \sum_{i=2}^{k} \left(1 - \frac{h_k}{2r_k}\right)^{-1}$$
$$\times \left\{ v^{t_{0i}}_{0(i-1)} \left(1 + \frac{h_{i-1}}{2r_{i-1}}\right) \left[ \prod_{j=i}^{k-1} \left(\frac{1+(h_j/2r_j)}{1-(h_j/2r_j)}\right)\right]\right\}$$

$$w^t_{0k} = \left[ w^t_{01} + \frac{h_1}{2}(\bar{\varepsilon}^t_{rr})_1 + \sum_{i=2}^{k-1} h_i(\bar{\varepsilon}^t_{rr})_i + \frac{h_k}{2}(\bar{\varepsilon}^t_{rr})_k \right] - \sum_{i=2}^{k} \left\{ w^{t_{0i}}_{0(i-1)} + \frac{h_{i-1}}{2}(\bar{\varepsilon}^{t_{0i}}_{rr})_{i-1} \right\} \tag{76}$$

where $\prod$ symbolizes the product operator. For purposes of computation the mandrel is divided into "layers". Obviously all these mandrel "layers" appear simultaneously at $t_{0m}$, so $u^{t_{0m}}_{0(k-1)} = v^{t_{0m}}_{0(k-1)} = w^{t_{0m}}_{0(i-1)} = (\bar{\varepsilon}^{t_{0m}}_{rr})_k = 0$ for $-M \leqslant k \leqslant 0$. Thus for the mandrel all the terms within the curly brackets in eqn (68) vanish. Hence the mandrel's displacement coefficients can be written as ($-M \leqslant k < 0$)

$$u^t_{0k} = u^t_{00}$$

$$v^t_{0k} = \left(1 + \frac{h_k}{2r_k}\right)^{-1} \left[ v^t_{00} \left(1 - \frac{h_0}{2r_0}\right) \prod_{j=k+1}^{-1} \left(\frac{1-(h_j/2r_j)}{1+(h_j/2r_j)}\right)\right]$$

$$w^t_{0k} = \left[ w^t_{00} - \frac{h_0}{2}(\bar{\varepsilon}^t_{rr})_0 - \sum_{i=k+1}^{-1} h_i(\bar{\varepsilon}^t_{rr})_i - \frac{h_k}{2}(\bar{\varepsilon}^t_{rr})_k \right]. \tag{77}$$

Equations (76) and (77) allow us to express the displacements in all the layers in terms of the displacements in one layer each for the composite and the mandrel.

The composite cylinder and the mandrel are in contact during winding, but they may separate during curing or the subsequent cooling. As long as the composite and the mandrel are in contact, eqn (67) is valid at the cylinder–mandrel interface ($k = 1$). By combining it with eqn (75) we find that

$$u^t_{01} = u^t_{00} - u^{t_{01}}_{00}$$

$$v^t_{01} = \left[ v^t_{00} \left(\frac{1+(h_0/2r_0)}{1-(h_1/2r_1)}\right)\right] - \left\{ v^{t_{01}}_{00} \left(\frac{1+(h_0/2r_0)}{1-(h_1/2r_1)}\right)\right\}$$

$$w^t_{01} = \left[ w^t_{00} + \frac{h_0}{2}(\bar{\varepsilon}^t_{rr})_0 + \frac{h_1}{2}(\bar{\varepsilon}^t_{rr})_1 \right] - \left\{ w^{t_{01}}_{00} + \frac{h_0}{2}(\bar{\varepsilon}^{t_{01}}_{rr})_0 \right\}. \tag{78}$$

*Strain–displacement relations*

Once the desired form of the proposed displacement functions has been arrived at, they must be converted into strains before they can be used in the strain energy density expressions. For an individual thin cylindrical layer $k$ inside the cylinder or the mandrel, we may use the following linearized strain–displacement relations, applicable to thin shells (Reddy, 1985)

$$
\begin{aligned}
(\varepsilon^t_{xx})_k - (\varepsilon^{t_0}_{xx})_k &= \frac{\partial \bar{u}^t_k}{\partial x} + z\frac{\partial \hat{u}^t_k}{\partial x} \\
(\varepsilon^t_{\theta\theta})_k - (\varepsilon^{t_0}_{\theta\theta})_k &= \frac{\partial \bar{v}^t_k}{\partial \theta} + \frac{\bar{w}^t_k}{r_k} + z\frac{\partial \hat{v}^t_k}{\partial \theta} \\
(\gamma^t_{\theta r})_k - (\gamma^{t_0}_{\theta r})_k &= \frac{\partial \bar{w}^t_k}{\partial \theta} + \hat{v}^t_k - \frac{\bar{v}^t_k}{r_k} \\
(\gamma^t_{rx})_k - (\gamma^{t_0}_{rx})_k &= \frac{\partial \bar{w}^t_k}{\partial x} + \hat{u}^t_k \\
(\gamma^t_{x\theta})_k - (\gamma^{t_0}_{x\theta})_k &= \frac{\partial \bar{v}^t_k}{\partial x} + \frac{\partial \bar{u}^t_k}{\partial \theta} + z\left[\frac{\partial \hat{v}^t_k}{\partial x} + \frac{\partial \hat{u}^t_k}{\partial \theta} + \frac{1}{2}\left(\frac{1}{r_k}\right)\left(\frac{\partial \bar{v}^t_k}{\partial x} - \frac{\partial \bar{u}^t_k}{\partial \theta}\right)\right].
\end{aligned}
\tag{79}
$$

Equation (79) together with eqns (76) and (77) yield the strains in terms of the unknown displacement coefficients

$$
\left.
\begin{aligned}
(\varepsilon^t_{xx})_k - (\varepsilon^{t_0}_{xx})_k &= u^t_{01} - \sum_{i=2}^{k} u^{t_{0(i-1)}}_{0(i-1)} \\
(\varepsilon^t_{\theta\theta})_k - (\varepsilon^{t_0}_{\theta\theta})_k &= \frac{1}{r_k}\left[w^t_{01} + \frac{h_1}{2}(\bar{\varepsilon}^t_{rr})_1 + \sum_{i=2}^{k-1} h_i(\bar{\varepsilon}^t_{rr})_i + \frac{h_k}{2}(\bar{\varepsilon}^t_{rr})_k\right] \\
&\qquad - \frac{1}{r_k}\sum_{i=2}^{k}\left\{w^{t_{0(i-1)}}_{0(i-1)} + \frac{h_{i-1}}{2}(\bar{\varepsilon}^{t_{0(i-1)}}_{rr})_{i-1}\right\} \\
(\gamma^t_{\theta r})_k - (\gamma^{t_0}_{\theta r})_k &= 0 \\
(\gamma^t_{rx})_k - (\gamma^{t_0}_{rx})_k &= 0 \\
(\gamma^t_{x\theta})_k - (\gamma^{t_0}_{x\theta})_k &= \left(\frac{1+\frac{3}{2}(z/r_k)}{1-(h_k/2r_k)}\right)\left\{v^t_{01}\left(1+\frac{h_1}{2r_1}\right) + \sum_{i=2}^{k-1} v^t_{0i}\left(\frac{h_i}{r_i}\right)\right. \\
&\qquad \left. - \sum_{i=2}^{k}\left[v^{t_{0(i-1)}}_{0(i-1)}\left(1+\frac{h_{i-1}}{2r_{i-1}}\right)\right]\right\}
\end{aligned}
\right\} \quad k \geqslant 1
\tag{80a}
$$

$$
\left.
\begin{aligned}
(\varepsilon^t_{xx})_k - (\varepsilon^{t_0}_{xx})_k &= u^t_{00} \\
(\varepsilon^t_{\theta\theta})_k - (\varepsilon^{t_0}_{\theta\theta})_k &= \frac{1}{r_k}\left[w^t_{00} - \frac{h_0}{2}(\bar{\varepsilon}^t_{rr})_0 - \sum_{i=k+1}^{-1} h_i(\bar{\varepsilon}^t_{rr})_i - \frac{h_k}{2}(\bar{\varepsilon}^t_{rr})_k\right] \\
(\gamma^t_{\theta r})_k - (\gamma^{t_0}_{\theta r})_k &= 0 \\
(\gamma^t_{rx})_k - (\gamma^{t_0}_{rx})_k &= 0 \\
(\gamma^t_{x\theta})_k - (\gamma^{t_0}_{x\theta})_k &= \left(\frac{1+\frac{3}{2}(z/r_k)}{1-(h_k/2r_k)}\right)\left[v^t_{00}\left(1-\frac{h_0}{2r_0}\right) - \sum_{i=k+1}^{-1} v^t_{0i}\left(\frac{h_i}{r_i}\right)\right]
\end{aligned}
\right\} \quad k \leqslant 0.
\tag{80b}
$$

The fiber's total strain may differ from the layer strains defined above. The longitudinal strain in the fibers, as used in this model, is obtained by linearizing eqn (35), which yields (Calius and Springer, 1989)

$$(\varepsilon_f^t)_k - (\varepsilon_f^{to})_k = \left(\frac{\partial u_k^t}{\partial x}\right)\cos^2\phi_{0k} + \left[\left(\frac{w_k^t}{r_k}\right) + \frac{(w_f^t)_k}{r_k}\right]\sin^2\phi_{0k} \tag{81}$$

where $(w_f^t)_k$ is provided by the Fiber Motion Submodel [eqn (41)]. On the other hand, in terms of its hoop and axial components, the longitudinal fiber strain can be defined as (Calius and Springer, 1989)

$$\begin{aligned}(\varepsilon_f^t)_k - (\varepsilon_f^{to})_k = {} & (\varepsilon_{f_{xx}}^t)_k \cos^2\phi_k - (\varepsilon_{f_{xx}}^{to})_k \cos^2\phi_{0k} + (\varepsilon_{f_{\theta\theta}}^t)_k \sin^2\phi_k - (\varepsilon_{f_{\theta\theta}}^{to})_k \sin^2\phi_{0k} \\ & + (\gamma_{f_{x\theta}}^t)_k \cos\phi_k \sin\phi_k - (\gamma_{f_{x\theta}}^{to})_k \cos\phi_{0k} \sin\phi_{0k}. \end{aligned} \tag{82}$$

During processing the change in fiber angle is small, so that $\phi_{0k} \simeq \phi_k$. With this approximation, comparison of eqn (81) and eqn (82) yields

$$\begin{aligned}(\varepsilon_{f_{xx}}^t)_k - (\varepsilon_{f_{xx}}^{to})_k &= \frac{\partial u_k^t}{\partial x} \\ (\varepsilon_{f_{\theta\theta}}^t)_k - (\varepsilon_{f_{\theta\theta}}^{to})_k &= \frac{w_k^t}{r_k} + \frac{(w_f^t)_k}{r_k} \\ (\gamma_{f_{x\theta}}^t)_k - (\gamma_{f_{x\theta}}^{to})_k &= 0. \end{aligned} \tag{83}$$

By comparing the above to eqns (63)–(79), it becomes possible to express the axial and hoop components of the total fiber strain as

$$\begin{aligned}(\varepsilon_{f_{xx}}^t)_k - (\varepsilon_{f_{xx}}^{to})_k &= (\varepsilon_{xx}^t)_k - (\varepsilon_{xx}^{to})_k \\ (\varepsilon_{f_{\theta\theta}}^t)_k - (\varepsilon_{f_{\theta\theta}}^{to})_k &= (\varepsilon_{\theta\theta}^t)_k - (\varepsilon_{\theta\theta}^{to})_k + \frac{w_f^t}{r_k}. \end{aligned} \tag{84}$$

As stated previously, the shear in the fibers is assumed to be negligible.

Inspection of eqns (80) and (84) reveals that all of the cylinder's and the mandrel's strain components are expressed in terms of the following six unknown displacement coefficients, which depend only on time

$$\boldsymbol{\Omega} = \{u_{00}^t, v_{00}^t, w_{00}^t, u_{01}^t, v_{01}^t, w_{01}^t\}. \tag{85}$$

When the cylinder and the mandrel are in contact there are only three unknowns

$$\boldsymbol{\Omega} = \{u_{01}^t, v_{01}^t, w_{01}^t\}. \tag{86}$$

The symbol $\boldsymbol{\Omega}$ represents the unknowns.

*Governing equations*

The variational problem posed by eqn (44) can now be evaluated in the following steps.

(i) Substitution of the strain–displacement relations [eqns (79)–(84)] into the stress–strain relations [eqns (56)–(61)] yields the stresses in terms of displacements.

(ii) Substitution of the resulting expressions for the stresses in the strain energy density definitions [eqns (53) and (55)] provides the strain energies in terms of displacements.
(iii) Substitution of the strain energy density terms in the variational equation [eqn (52)], followed by
(iv) Variation of the resulting expression with respect to each of the unknowns in $\Omega$ [eqn (85) or (86)], produces a set of algebraic equilibrium equations.

The governing equations produced by this procedure are rather long (Calius and Springer, 1989). Solution of these equations yields the values for the $\Omega$ unknowns at any instant of time. Once these values are known, the strains and the stresses can readily be determined from the strain–displacement [eqn (80)] and stress–strain [eqns (56), (60) and (61)] relations.

Solutions must be found through a numerical procedure. The numerical algorithms which were used in this study are discussed subsequently.

## 6. VOID GROWTH SUBMODEL

The void submodel provides the size of a void at a given location in the composite as a function of time. The analysis employed is the same as that proposed by Springer and Loos for the growth of voids in laminated composites made of prepreg tape. Details of the analysis are given in Springer (1983) and Loos and Springer (1983).

## 7. STRENGTH SUBMODEL

There is no generally accepted method available for calculating the strength of composite cylinders, especially while the composite material is undergoing changes during processing. To estimate failures in the cylinder we relied on failure criteria. These criteria are based on quasi-empirical methods of estimating the strength of each layer in the cylinder. The following four methods were incorporated into the model: (i) the maximum stress criterion, (ii) the maximum strain criterion, (iii) the Tsai–Wu quadratic criterion in stress space, and (iv) the Tsai–Wu quadratic criterion in strain space. The equations relevant to each of the criterion can be found in Calius and Springer (1989) and Tsai (1987).

## 8. METHODS OF SOLUTION

Solutions to the filament winding process model must be obtained by numerical methods. In the following we briefly summarize the methods we applied to the solution of the various submodels. It is emphasized that the different submodels are interconnected and the solutions must be computed simultaneously.

Solutions to the energy equation [eqn (1)], which forms the basis of the model, were generated by a standard combination of finite-element and finite-difference methods Zienkiewicz (1977). The finite-element formulation transforms the energy equation into a set of first-order ordinary differential equations with variable coefficients in the time domain. This set of differential equations was reduced to a set of linear algebraic equations by a finite-difference formulation which marches through the process in a sequence of time steps. The equation coefficients are taken to be constant during each time step. The time step size is not constant but varies, under the algorithm's control, throughout the process.

The finite-difference equations were formulated using a two-point implicit finite-difference scheme. The procedure was developed in general form so that forward, backwards, Crank–Nicolson or Galerkin methods could be used. All these options were incorporated to allow the user to trade off time step size, which strongly influences computational speed, for computational stability, according to the characteristics of the problem. In general, the Crank–Nicolson scheme was found to be satisfactory.

Although the coefficients of the resulting set of algebraic equations make up a tridiagonal matrix, the conventional tridiagonal solver algorithms were not used because

of numerical instabilities. Instead, solutions were obtained by Gaussian elimination with partial pivoting, as implemented for banded matrices by the DGBCO and DGBSL subroutines of the LINPACK library (Dongarra *et al.*, 1979).

The equation pertaining to the stress–strain submodel constitute a set of linear algebraic equations. Solutions to these equations at the end of each Thermochemical Submodel time step were obtained by Gaussian elimination with partial pivoting method, as implemented by the DGECO and DGESL subroutines of the LINPACK library (Dongarra *et al.*, 1979).

Solutions to the partial differential equation describing vapor diffusion to and from the voids were obtained by an explicit finite-difference scheme (Carnahan *et al.*, 1969).

The Fiber Motion and Failure Submodels are represented by simple algebraic equations which can be evaluated in a straightforward manner at the end of each time step.

An algorithm was developed which incorporated the aforementioned submodel solution methods. This algorithm was implemented in a computer code named WIND. (This code may be obtained from the authors.) The input parameters required by the code and the output provided by the code are discussed in Lee and Springer (1989).

## 9. CONCLUDING REMARK

The model described in this paper relates the thermal, chemical and mechanical behavior of filament wound thin cylinders to the three process variables: winding speed, fiber tension, and ambient temperature. Verification of the model and illustration of the use of the model in the selection of the proper process variables are given in two companion papers (Calius *et al.*, 1989; Lee and Springer, 1989).

*Acknowledgements*—This work was supported by David Taylor Ship R&D Center and by NASA Marshall Space Flight Center.

## REFERENCES

Bhi, S. T., Hansen, R. S., Wilson, B. A., Calius, E. P. and Springer, G. S. (1987). Degree of cure and viscosity of Hercules HBRF-55 resin. *Advanced Materials Technology '87*, Society for the Advancement of Materials and Process Engineering, **32**, 1114–1118.

Boyce, W. E. and DiPrima, R. C. (1977). *Elementary Differential Equations*, Chapter 2. John Wiley, New York.

Calius, E. P., Lee S. Y. and Springer, G. S. (1989). Filament winding cylinders: II. Experimental results. *J. Composite Mater.* (submitted).

Calius, E. P. and Springer, G. S. (1989). Simulation of filament winding thin cylinders. Report to David Taylor Ship R&D Center, Annapolis; also Calius, E. P., Ph.D. Thesis, Department of Aeronautics and Astronautics, Stanford University.

Calladine, C. R. (1986). *Theory of Shell Structures*, Chapter 6. Cambridge University Press, U.K.

Carnahan, B., Luther, H. A. and Wilkes, J. O. (1969). *Applied Numerical Methods*. Chapter 7. John Wiley, New York.

Collins, R. E. (1961). *Flow of Fluids through Porous Materials*. Chapter 3. Rheinhold. Scarborough, CA.

Daily, J. W. and Harleman, D. R. F. (1966). *Fluid Dynamics*, Chapter 9-3. Addison Wesley, Reading, MA.

Dongarra, J. J., Bunch, J. R., Moler, C. B. and Stewart, G. W. (1979). LINPACK User's Guide, Chapters 1 and 2.

Dusi, M. R., Lee, W. I., Ciriscioli, P. R. and Springer, G. S. (1987). Cure kinetics and viscosity of Fiberite 976 resin. *Composite Mater.* **21**, 243–261.

Eckert, E. R. G. and Drake, R. M., Jr. (1972). *Analysis of Heat and Mass Transfer*, Chapter 1. McGraw-Hill, Scarborough, CA.

Happel, J. (1959). Viscous flow relative to arrays of cylinders. *AICHE Jl* **5**, 174–177.

Jones, R. M. (1975). *Mechanics of Composite Materials*, Appendix A. Scripta, Washington, D.C.

Lanczos, C. (1986). *The Variational Principles of Mechanics*, Chapter 2. Dover, New York.

Lee, S. Y. and Springer, G. S. (1989). Filament winding cylinders: III. Selection of the process variables. *J. Composite Mater.* (submitted).

Lee, W. I., Loos, A. C. and Springer, G. S. (1982). Heat of reaction, degress of cure, and viscosity of Hercules 3501-6 resin. *J. Composite Mater.* **16**, 510–520.

Loos, A. C. and Springer, G. S. (1983). Curing of epoxy matrix composites. *J. Composite Mater.* **17**, 135–169.

Lubin, G. (Ed.) (1982). *Handbook of Composites*, Chapter 16. Van Nostrand Rheinhold, Scarborough, CA.

Reddy, J. N. (1985). *Energy and Variational Methods in Applied Mechanics*, Chapters 2 and 4. John Wiley, New York.

Springer, G. S. (1983). A model of the curing process of epoxy matrix composites. In *Progress in Science and Engineering of Composites* (Edited by T. Hayashi, K. Kawaka and S. Umekawa), pp. 23–35. Japan Society for Composite Materials, Tokyo, Japan.

Tsai, S. W. (1987). *Composites Design*, Sections 3, 4, 5 and 11. Think Composite. Dayton, Ohio.

Zienkiewicz, O. C. (1977). *The Finite Element Method*, Chapters 20 and 21. McGraw-Hill, Scarborough, CA.

## APPENDIX A: VARIATION OF PROPERTIES WITH DEGREE OF CURE

The density $\rho$, the heat conductivity $k$ and the heat capacity per unit volume $C'$ of the resin are related to the degree of cure $\alpha$ by the following simple linear relationships

$$\rho_r = \alpha\rho_r^c + (1-\alpha)\rho_r^{uc} \tag{A1}$$

$$k_r = \alpha k_r^c + (1-\alpha)k_r^{uc} \tag{A2}$$

$$C_r' = \alpha C_r'^c + (1-\alpha)C_r'^{uc}. \tag{A3}$$

The following piecewise linear relations were used to represent the mechanical properties of the composite

$$\begin{aligned} Y &= Y^{uc} && \alpha \leqslant \alpha_0 \\ Y &= \bar{\alpha}Y^c + (1-\bar{\alpha})Y^{uc} && \alpha_0 < \alpha < \alpha_1 \\ Y &= Y^c && \alpha_1 \leqslant \alpha \end{aligned} \tag{A4}$$

where $Y$ represents the composite Young's moduli $E$, shear moduli $G$, or Poisson's ratios $v$. The ratio $\bar{\alpha}$ is defined as

$$\bar{\alpha} = \frac{\alpha - \alpha_0}{\alpha_1 - \alpha_0} \tag{A5}$$

where $\alpha_0$ and $\alpha_1$ are the values $\alpha$ at which the "hardening" of the resin starts and ends. The superscripts u and uc refer to the properties of the cured ($\alpha = 1$) and uncured ($\alpha = 0$) resin. The above properties vary with time since the degree of cure varies with time.

## APPENDIX B: FIBER MOTION SUBMODEL

Solutions to eqn (36) can be expedited by observing that some of the terms are negligible when considering the change in fiber position $w_f$ over a small time interval $\Delta t$. Substraction of the equilibrium equation at $t-\Delta t$ from that at $t$ results in an incremental form of the equilibrium equation

$$f_3^t\dot{w}_f^t + \frac{w_f^t}{R_f^0}\dot{w}_f^t + f_2^t\frac{w_f^{t^2}}{R_f^{0^2}} + f_1^t\frac{w_f^t}{R_f^0} + f_0^t - f_3^{t-\Delta t}\dot{w}_f^{t-\Delta t} - \frac{w_f^{t-\Delta t}}{R_f^0}\dot{w}_f^{t-\Delta t} - f_2^{t-\Delta t}\frac{w_f^{t-\Delta t^2}}{R_f^{0^2}} - f_1^{t-\Delta t}\frac{w_f^{t-\Delta t}}{R_f^0} - f_0^{t-\Delta t} = 0 \tag{B1}$$

where the superscripts $t$ and $t-\Delta t$ denote values evaluated at those particular times. We define the fiber displacement increment as

$$\Delta w_f = w_f^t - w_f^{t-\Delta t} \tag{B2}$$

$$\frac{d(\Delta w_f)}{dt} = \dot{w}_f^t. \tag{B3}$$

Equation (B1) may then be rearranged to yield

$$g_3^t\Delta\dot{w}_f + \frac{\Delta w_f}{R_f^0}\Delta\dot{w}_f + g_2^t\frac{\Delta w_f^2}{R_f^{0^2}} + g_1^t\frac{\Delta w_f}{R_f^0} + g_0^t = 0 \tag{B4}$$

where the parameters $g_0$ through $g_3$ are given by eqn (40).

Upon examination of eqn (37) it is apparent that the orders of magnitude of the parameters $f_0$ through $f_3$ are

$$O(f_3) \simeq O(1), \quad O(f_2) \simeq CO(1), \quad O(f_1) \simeq CO(1), \quad O(f_0) \simeq CO(\lambda) \tag{B5}$$

where $\lambda$ is a very small number compared to unity.

The total fiber displacement at the start of the increment $w_f^{t-\Delta t}$ is small compared to $R_f^0$, hence

$$O\left(\frac{w_f^{t-\Delta t}}{R_f^0}\right) \simeq O(\lambda).$$

Furthermore, for "slow" fiber motion it is assumed that

$$O\left(\frac{\dot{w}_f^{t-\Delta t}}{C}\right) \simeq O(\lambda).$$

Then the orders of magnitude of the parameters $g_0$ through $g_3$ are

$$O(g_3) \simeq O(1), \quad O(g_2) \simeq CO(1), \quad O(g_1) \simeq CO(1), \quad O(g_0) \simeq CO(\lambda). \tag{B6}$$

Thus eqn (B4) becomes

$$O(1)\frac{\Delta\dot{w}_f}{C} + \frac{\Delta w_f}{R_f^0}\frac{\Delta\dot{w}_f}{C} + O(1)\frac{\Delta w_f^2}{R_f^{0^2}} + O(1)\frac{\Delta w_f}{R_f^0} + O(\lambda) = 0 \tag{B7}$$

where the increments $\Delta w_f$ and $\Delta\dot{w}_f$ during a small time interval $\Delta t$ are considered to be of the same order of magnitude as $w_f^{t-\Delta t}$ and $\dot{w}_f^{t-\Delta t}$. Hence $O(\Delta w_f/R_f^0) \simeq O(\lambda)$ and $O(\Delta\dot{w}_f/C) \simeq O(\lambda)$. The second and third terms in eqn (B7) are clearly of higher order than the rest and can be neglected, and eqn (B4) reduces to eqn (39) in the text.

## APPENDIX C: STIFFNESS AND THERMAL EXPANSION COEFFICIENTS

The reduced stiffness matrix $[\bar{Q}]$ for a cylindrical layer is defined in the $(x, \theta, r)$ coordinate system. The stiffness matrix $[Q]$ of the material in this layer is defined in the material's on-axis coordinates (1, 2, 3). The $[\bar{Q}]$ and $[Q]$ stiffness matrices are related by

$$[\bar{Q}] = [J]^{-1}[Q][J^T]^{-1} \tag{C1}$$

where $[J]$ is the layer's transformation matrix (Tsai, 1987; Jones, 1975). We assume that the material is transversely isotropic. Then, the nonzero elements of the stiffness matrix $[Q]$ are

$$\begin{aligned}
Q_{11} &= \frac{E_{11}}{1-\nu_{12}\nu_{21}} \\
Q_{22} &= \frac{E_{22}}{1-\nu_{12}\nu_{21}} \\
Q_{12} = Q_{21} &= \frac{\nu_{12}E_{11}}{1-\nu_{12}\nu_{21}} \\
Q_{23} = Q_{32} &= \frac{(\nu_{23}+\nu_{12}\nu_{21})E_{22}}{(1+\nu_{23})(1-\nu_{23}-2\nu_{12}\nu_{21})} \\
Q_{66} &= E_{66}
\end{aligned} \tag{C2}$$

where

$$\nu_{21} = \nu_{12}(E_{11}/E_{22}). \tag{C3}$$

$E_{ii}$ and $\nu_{ij}$ $(i \neq j)$ are the moduli and Poisson's ratios. The subscripts $i$ and $j$ refer to the longitudinal $(i,j = 1)$, transverse $(i,j = 2,3)$ and shear $(i,j = 6)$ components when using contracted notation.

By manipulating Hooke's law in the material's on- and off-axis coordinates, it can be shown (Calius and Springer, 1989) that the composite stiffness coefficients at $t_0$ are

$$\begin{aligned}
(S_f'^0) &= \left[\left(Q_{11} - \frac{Q_{12}}{Q_{22}+Q_{23}}\right)^{-1}\right]^{t_0} \\
(S_T'^0) &= \left[-\frac{Q_{12}}{Q_{22}+Q_{23}}\right]^{t_0}(S_f'^0).
\end{aligned} \tag{C4}$$

In the cylindrical coordinate system the nonzero components of the thermal expansion coefficients $\beta$ are

$$\begin{aligned}
\beta_{xx} &= \beta_{11}\cos^2\phi + \beta_{22}\sin^2\phi \\
\beta_{\theta\theta} &= \beta_{11}\sin^2\phi + \beta_{22}\cos^2\phi \\
\beta_{x\theta} &= 2(\beta_{11}-\beta_{22})\sin\phi\cos\phi
\end{aligned} \tag{C5}$$

where $\beta_{ii}$ are the on-axis coefficients of the thermal expansion coefficients.

Note that the engineering constants ($E$ and $\nu$) and the on-axis thermal expansion coefficients ($\beta$) vary with the degree of cure (Appendix A). These properties change with time because of changes in the degree of cure with time.